1. INTRODUCUCTION

This report describes the design, construction and preliminary testing of a new high-accuracy star-tracking telescope for the laboratory model of the Stanford Gyro Relativity Experiment. The function of the telescope in the final flight experiment is to define (by reference to a suitable star) a direction in space for comparison with the relativistic precession of a group of gyroscopes. The design of the telescope has been strongly affected by, and has in turn influenced, designs for other portions of the overall experiments, for example the gyroscopes, the attitude control system of the satellite, and the instrumentation system used in processing relativity data. With the constraints so imposed, the following have been the main goals for the star-tracker:

(a) independent readout of angular position in two planes, orthogonal to each other and aligned with the gyro readout planes to within 10 arc-seconds or better.

(b) absolute null stability over a one year period of mechanical parts and readout to 0.001 arc-second.

(c) readout linear to 0.001 arc-seconds over ± 0.05 arc-second, and having an acquisition range of ± 2 arc-minutes.

(d) noise performance leading to a resolution of 0.05 arc-second in 0.1 second observation time of the chosen reference star (probably Rigel), and capable of integration to 0.001 arc-second over a longer period.

(e) provision for automatic gain control, referred to the gyroscope, capable of matching the gains of the gyroscopes and telescope readouts to 1% or better.

Some of these requirements are nearly three orders of magnitude higher than the best performance now obtained with star-trackers operating on earth. The hope for such a large improvement comes from the combination of space flight with the cryogenic techniques which are also required elsewhere in the experiment. Broadly the factors limiting telescopes on earth are three: (1) atmospheric turbulence, (2) distortion and creep of the structure under its own weight, (3) distortion due to differential thermal expansion. Operation in space solves the first two; operation at liquid helium temperatures solves the third. However one cannot reap the potential improvements merely by taking an existing star-tracker and putting it in liquid helium. Many other points have to be taken into consideration, as will appear below.

The design of the star-tracker is due chiefly to C. W. F. Everitt and R. A. Van Patten of Stanford University and D. E. Davidson of Davidson Optronics Company, at whose plant the parts have been made. Figure 1 shows the main features. The telescope has folded Schmidt-Cassegrain optics, with 150 inch focal length and 5 1/2 inch aperture. The physical dimensions are: overall length 14 inches, outside diameter 7 1/4 inches. The parts are made entirely of fused quartz, held together by "optical contacting", that is, by direct molecular adhesion of the quartz surfaces. No cements or mechanical attachement devices are used. The one unconventional feature of the optical layout is that the light path is folded to put the focal plane just above the corrector plate instead of below the primary mirror as in the standard Cassegrain

telescope. This has three advantages: (1) it leaves the bottom surface of the telescope clear for attaching gyro components, (2) it reduces the physical length of the telescope needed for a given focal length. The last advantage is one of practice rather than principle. Theoretically there is no limit to the focal length of a Cassegrain/telescope. It is simply a question of choosing the right magnification ratio. However in practice there is a limit, because difficulties in making the secondary mirror mean that any increase in focal length beyond a certain point causes a deterioration of image quality. Having an extra stage of magnification eases the problem.

Angular readout is obtained as follows. A beam-splitter, located about an inch in front of the focal plane, forms two star images, one for each readout axis. Each image then falls on the sharp edge of a roof prism where it is again subdivided into two half images. Measurements of their relative intensities determine the angles between the two readout planes and the line of sight to the star. Practical consideration underlie the choice of two roof prisms.rather than a four sided pyramid to divide the image. To make a precise enough pyramidal divider, or other simple structures for quartering the image, is a hopeless task. Section 2 below gives a formula to determine the manufacturing tolerances for the prisms, as well as other formulae for effects of aperture, focal lengths and image size on the linearity and noise performance of the star-tracker.

The beam splitter and roof prisms are optically contacted into a "light-box" mounted in the middle of the corrector plate just over the central obscuration due to the secondary mirror. Lenses attached

to the light-box collimate the beams, which pass to small 45° mirrors at the side of the telescope and thence via light pipes to detectors at room temperature. The two axes have independent detection systems, comprised of a photomultiplier and chopping wheel so arranged that the signals from the paired light-pipes are presented successively on the same area of the photocathode. The chopping frequency is 50 Hz. In this way zero drift due to aging of the cathode material is avoided. The signals are amplified and synchronously demodulated in a circuit which includes an automatic gain control and other special features described in section 3.3 below. The separation of the two readout channels simplifies the design of the light-choppers and circuitry, eliminating the quadrature signals (of either optical or electronic origin) that might occur if all four signals were processed in a single chopper-detector.

Careful consideration was given to other readout schemes. There are attractions in methods which chop the image at the focal plane, for example, by a small vibrating reed or a rotating half disc mounted in the light-box. Such devices avoid the null offset that would occur with the scheme proposed here if the transmissibility of the light-pipes varies. But the objections are severe. Focal plane choppers introduce undesirable complications into the cryogenic environment and have null offsets of their own which are likely to be much larger than anything found here. The point is covered further in section 2.2 A possible improvement on the present scheme is to replace the light-pipes by periscopic image tubes. With good design these might improve both the null stability and optical efficiency of the telescope.

We intend to pursue the idea later.

Development of this star-tracking telescope was begun in 1966 under NASA Grant NSG-582 (now NGR 05-020-019). The work done under that Grant included experiments on the detection system using a model telescope and artificial star at room temperature, and a design lay-out of the optics. The scope of the present Contract from NASA Marshall Center has been to construct and test the actual telescope for the laboratory experiment at Stanford. For completeness this Report covers work pertinent to the whole program, including the preliminary experiments.

Testing the telescope to full precision in the laboratory is a difficult - perhaps an impossible - task. No adequate test equipment has ever been built. The performance checks described here cover several distinct aspects of the problem. With the calculations they give good hope that the design goals may be achieved. A plan for further tests, utilizing the gyroscopes and an artifical star, has been sketched out. It is described in section 6.

2. THEORETICAL CONSIDERATIONS

2.1 Optical Performance

Let the power flux from the star be S watt/cm^2. Then the total quantity of light entering a telescope of clean aperture D is $\pi s D^2/4$. Assume that a proportion $(1 - \alpha)$ of the aperture is obscured by the secondary mirror, that the efficiency of light-transmission through the optics is $\beta (0 < \beta < 1)$, and that the ratio of on-time to

off-time of the light-chopper is γ (~ 0.5), then the mean power level at each detector is

$$E = \frac{\pi}{8} \alpha\beta\gamma S D^2 \qquad (1)$$

the additional factor of $1/2$ being due to having two separate star images.

Consider an idealized telescope without a central obscuration ($\alpha = 1$). Assume further that the roof prisms are deliberately displaced from the focal plane, so that the effective image is a uniformly illuminated disc of diameter d much greater than the diameter d' of the diffraction image. The roof prism divides the disc into two areas A and B, and the readout consists in measuring the difference in power levels between A and B. Then from the geometry of the circle the difference ϵ due to a displacement S if the image is

$$\epsilon = \beta\gamma S D^2 \left(\frac{\delta}{d}\right) \left\{1 - \frac{2}{3}\frac{\delta^2}{d^2} + \frac{28}{15}\frac{\delta^4}{d^4}\right\} \qquad (2)$$

where δ and d are expressed in similar units of linear or angular measure. Defining the sensitivity σ as ϵ/δ, expressing δ and d in arc-secs and neglecting all terms except the first

$$\sigma = \beta\gamma S D^2/d \text{ watts/arc-sec} \qquad (3)$$

Equations (2) and (3) show that for a telescope with clear aperture defocussing reduces the sensitivity in direct proportion to the image diameter d, but improves the linearity over a given range in proportion to $1/d^2$.

Consider now a Cassegrainian telescope, still operating with a defocussed image, and having a circular central obscuration of diameter c. Then the bracketed term in equation (2) assumes the form

$$\left\{ 1 + \frac{2}{3}\,\delta^2 \left(\frac{1}{c^2} - \frac{1}{d^2}\right) - \frac{28}{15}\,\delta^2 \left(\frac{1}{c^4} - \frac{1}{d^4}\right) + \ldots \right\}$$

and since $c \sim 0.4d$ it is the obscuration rather than the aperture that is the main cause of nonlinearity. However the formula suggests a method of compensating the errors. If instead of the circular obscuration, a barrel shaped one is used, with axes parallel to the readout planes and edge curvature equal to d, then for displacement smaller than the barrel width c', all higher order terms in the bracket vanish, and the readout has perfect linearity over a range $\pm c'/2$. The analysis ignores diffraction effects. Some experiments done in the course of the preliminary research with the simulator confirmed that the linearity of a defocussed telescope is changed by shaping the obscuration. The results were limited by imperfections in the simulation optics. Probably the best approach to corrections of this kind is trial and error, using a series of obstacles of progressively different shape. In the actual telescope it is desirable, for reasons which are summarized below, to operate with a focussed image and diffraction

limited optics. Even so some improvement in linearity may be possible by playing with the shape of the obstacle; and this we intend to try.

Reverting to equation (2) for a clear aperture telescope, it is evident that the range of linear operation is fixed by the second term in the bracket. If Δ is the maximum acceptable departure from linearity (for the present telescope specified as 0.001 arec-second) and R the maximum allowed range, then from (2) ,

$$R = \pm 1.15 \cdot \Delta^{1/3} \quad d^{2/3} \qquad (4)$$

where R, Δ and d are expressed in similar units of linear or angular measure. Applying (4) to a circular disc equal in diameter to the diffraction image for green light in a 5 1/2 inch aperture telescope (d = 0.9 arc-second) one finds $R \sim \pm 0.1$ arc-second. An exact linearity formula for a diffraction limited image has been derived by W. L. Pondrom, Jr. The results obtained from it by R. Woodruff are given in figure 2. In this case the allowed motion is ± 0.6 arc-seconds for monochromatic light. The data shows that a telescope with 0.05 cm. second range can be made, allowing if necessary a small amount of defocussing.

The ultimate limit to precision of the star tracker is set by fluctuation in energy in the two halves of the image due to random arrivals of photons. To attain the limit, other sources of noise must be eliminated by suitable choice of detectors and amplifiers. Since this is a random noise problem, the final resolution of the system is proportional to $t^{-1/2}$ where t is the time of the measurement. An exact calculation would be extremely

elaborate, since it requires integrations over the photon spectrum of the star, the intensity distribution in the diffraction pattern, and the quantum efficiency of the photo detector for different wavelengths. A useful approximate idea is got by assuming an average wavelength $\bar{\lambda}$ corresponding to the color temperature of the star. Since the energy of a photon is hc/λ the average number of photons arriving at each detector in time t is

$$n = E \bar{\lambda} t/hc$$

The actual quantum noise depends not on the number of photons but the number of photoelectrons released at the cathode, that is $\overline{n \eta}$, where η is the quantum efficiency of the detector. The resultant random fluctuations ϵ_v between the two halves of the image are therefore $E/\sqrt{n \eta}$ or

$$\bar{\epsilon}_v = \frac{Ehc\bar{\nu}}{\bar{\lambda}\,\bar{\eta}}$$

where $\bar{\nu}$ is the bandwidth of the receiver (that is the reciprocal of t). With numerical values for h and c this becomes

$$\bar{\epsilon}_v = 4.48 \times 10^{-12} \sqrt{\frac{E\,\bar{\nu}}{\bar{\lambda}\,\bar{\eta}}} \quad . \qquad (5)$$

For a defocussed telescope with a central obscuration of diameter C, the sensitivity equation (3) assumes the form

$$\sigma = \beta \gamma S (D - C)^2/d \qquad (3a)$$

$$\sigma = 1.07 \ \alpha\beta\gamma \ S \ D^2/d' \qquad (3b)$$

The energy flux S is related to stellar magnitude M by

$$S = 2.83 \times 10^{-12}(2.51)^M \text{ watts/cm}^2 \qquad (6)$$

Define a noise equivalent angle $\bar{\delta}_\nu = \epsilon\nu/\sigma$. Then combining equations (1), (3a), (5), (6) and observing that α for a circular obscuration is $1 - \frac{c^2}{D^2}$ one finds after some manipulation that the noise equivalent angle for a defocussed telescope is given

$$\bar{\delta}_\nu = 1.67 \times 10^{-6} \ \frac{d}{D} \ \left(1 + \frac{c}{D}\right)^2 \ \sqrt{\frac{2.51^M \ \bar{\nu}}{\bar{H} \ \bar{\lambda}}} \qquad (7)$$

where $\bar{H} = \beta \ \gamma \ \bar{\eta}$ is defined as the total optical efficiency of the star-tracker. The analogous result for a focussed telescope with diffraction limited optics is found using equations (3b) and substituting for d' from the Airy formula $d' = 1.22 \ \bar{\lambda}/D$. The result is

$$\bar{\delta}_\nu = 2.05 \times 10^{-6} \ \frac{1}{D^2} \ 1 + \frac{c^2}{2D^2} \ \sqrt{\frac{2.51^M \bar{\nu} \ \bar{\lambda}}{\bar{H}}} \ . \qquad (8)$$

Equation (6) shows that the noise fluctuations increase linearly as the image is defocussed. The resolution improves with increasing aperture in proportion to D^2 for the diffraction limited image and

D for the out of focus image. In both cases the resolution is improved by increasing the optical efficiency $\bar{H}$ and the integration time τ ($= 1/\bar{\nu}$) . It is also improved by having small M , and in the diffraction limited case small $\bar{\lambda}$ as well, choosing, that is, a bright blue star.

For Rigel M = 0.7 and $\bar{\lambda}$ is 5×10^{-5} cm . With D as 5 1/2 inch (14 cm) and C 2.2 inch (5.7 cm) the number of photons entering the telescope per second is about 3×10^{8} . With $\beta = 0.1$, $\bar{\eta} = 0.05$, $\gamma = 0.5$ the total optical efficiency $\bar{H}$ is about 2.5×10^{-3} . For a diffraction limited image the resolution is then 4×10^{-3} arc-seconds in 0.01 seconds of integration time. The diameter of the diffraction image is 0.9 arc-second. A defocussed image of 10 arc-second diameter gives a resolution of 6×10^{-2} arc-second in the same 0.01 second integration time.

To avoid rectification errors the telescope must be kept pointed within the acceptable range of motion derived from equation (4). The fundamental limit to pointing accuracy is evidently the noise in the telescope output at the bandwidth of the attitude control system. New equation (4) shows that R varies as $d^{2/3}$ the defocussed image diameter, while equation (6) shows that $\bar{\delta}_{\nu}$ varies as d . For a star of given brightness there is accordingly a limit to the amount of defocussing that can be accepted, having the form

$$d_{max} < 2.6 \times 10^{17} \frac{D^3}{\left(1 + \frac{e}{D}\right)^6} \left(\frac{\bar{H}\,\bar{\nu}}{2.51^{M}\,\bar{\nu}}\right)^{3/2} \Delta \qquad (9)$$

where again Δ is the acceptable nonlinearity. With the existing design of control system and choice of reference star, the performance is well within the limit for all conceivable amounts of defocussing, but considerations of this kind begin to be critical for stars fainter than 5th magnitude.

The photon noise formulae give the fundamental limit to telescope performance. There are also practical limits if the dividing edges of the roof prisms are chipped, or curved along the roof line, or are not orthogonal to each other. Formulae for these errors were derived first by R. A. Nidey. The effects of ridge curvature are negligible. A formula for the effects of nicks, somewhat different from Dr. Nidey's may be obtained from the following considerations. Recall first that the only kind of error that counts is a change in position of the null during the course of the year. Thus with a star image which approximates to a uniformly illuminated disc, there is no reference error so long as the nick always lies inside the disc. The trouble comes when cross-axis motions of the beam along the roof line bring new nicks in or out of the image. Call the total cross axis range of motion $2R'$. The worst error comes where an elongated chip on one prism face, of width ω, enters the disc. The resultant null shift Δ is $R'\omega/d$ where d is again the image diameter. But from equation (4) the maximum acceptable range of motion R is related to the maximum allowed error Δ by $R^3 = 1.5\,\Delta d^2$. Taking $R = R'$, eliminating d and multiplying by focal length to convert from angular to linear size, one has as the maximum acceptable chip width

$$\omega < 0.81\, R^{1/2}\, \Delta^{1/2}\, f \qquad (10)$$

With f as 150 inches, R as 0.05 arc-seconds, equation (10) gives a maximum width of 13 microinches. This is the limit when the length of the chip exceeds $2Rf$, that is, about 80 microinches. For shorter chips the width can be greater. Prisms have already been made with no chips more than 5 microinches across.

The maximum allowed departure from orthogonality in the two roof lines is

$$\phi < \Delta/2R \qquad (11)$$

which gives a maximum ϕ of 0.5° for R equal to 0.05 arc-seconds. In practice there are more stringent requirements set by problems in gyro referenceing, and the parts are aligned to within 10 arc-seconds.

Further conclusions from the formulae derived here are summarized in section 3.1 .

2.2 Mechanical and Cryogenic Considerations

The most important of the mechanical considerations affecting telescope design is also the simplest. An angle of 0.001 arc-seconds is 5×10^{-9} radians. Subtended over the focal length of the telescope this is a linear displacement of 0.75 microinches; subtended over the diameter of the primary mirror it is 0.015 microinches, or about 4 Å . The difficulty of modulating the image at the focal plane is obvious at once. Consider a rotating knife-edge image-chopper. The axis of rotation would have to be held constant over the course of a year to better than 0.75 microinches; and that in high vacuum at a temperature of 2 to 4 K. Two types of bearing might in principle be applied to the task: magnetic,

with superconducting support pads, or electric, with condenser plates to which voltages are applied by a dynamical suspension system similar to the one used now in the relativity gyroscopes. For the gyroscope suspension, with a 1.5×10^{-3} inch gap between the rotor and housing, the best long-term centering stability achieved so far (in the new Stanford/MSFC system) is 25 microinches. An improvement is possible by reducing the gap. The minimum practical to work with in a cylindrical geometry is about 1.5×10^{-4} inches. Since the system scales linearly the best stability that can be hoped for is 2.5 microinches. Thus errors of 0.004 arc-second or more over the year ar to be expected with an electrical suspension. Superconducting bearings with comparable tolerances have never been built. Some work on that problem is now being done at Stanford.

The possibilities for a vibrating reed chopper in the focal plane have been examined by W. L. Pondrom, Jr. The best approach seems to be to have two orthogonally mounted quartz filaments of dimensions comparable to the image diameter, driven electrically at different frequencies. The filaments could be left attached to the rods from which they are drawn; these would then be optically contacted to the light box. A device of this kind should have excellent linearity and resolution . But there are still null problems. It is commonly said that the equilibrium position of a vibrating mechanical system is as good as that of a stationary system. Often that may be true, but at the level of precision needed here the statement may te taken with a large pinch of salt. For the null point moves through the relaxation of asymmetric strains in the filament.

Ordinarily such delayed elastic processes are thermally activated, but here the vibrational energy is about 10^8 times the thermal noise, and so may be expected to generate much bigger null shifts than occur in the non-vibrating system. The subject is one that owes more to guesswork than measurement, but the idea seems to be borne out by analogy with other activation processes. For example vibration of an iron sheet in the earth's magnetic field induces an anhysteretic magnetization many times larger than the static magnetization acquired in the same field. Another source of trouble in the vibrating reed detector is stray electric charges, which again cause a shift in the null point. Possibly the errors could be eliminated by an auxiliary reference system to measure the position of the reed with respect to a fixed line on the quartz telescope structure.

The restriction to 4 Å of motion over the diameter of the primary mirror sufficiently indicates the problems encountered elsewhere. It shows at once how important the optical contacting technique is in constructing a stable telescope. Consider the alternative of conventional adhesives, say an epoxy cement. Over the course of a year differential shrinkage due to aging may easily exceed 1% . But the thinnest layers of epoxy are more than 1000 Å . Thus motions of 10 Å or more are almost bound to occur, introducing errors several times larger than the acceptable limit. Experiments on optical contacting are reported in section 5.

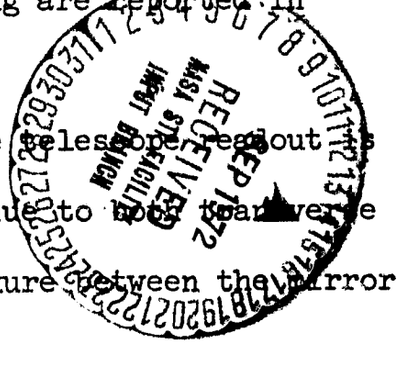

In a gravitational field the null point of the telescope readout is affected by elastic deformation of the structure, due to both transverse displacement of the image dividers and angular flexure between the mirror

surfaces. Transverse displacements of the secondary mirror also cause aberrations which affect both the linearity and null position. When a horizontal telescope, cantilevered from one end, is rotated about its optic axis, the image position varies sinusoidally with orientation. Let F be the local acceleration (which on earth is equal to g) and θ_Y the maximum resultant angular error in readout. Then applying the standard formulae for flexure and displacement of a heavy centilevered tube with a finite mass (the corrector plate and attachments) at the free end, one has

$$\theta_Y = \frac{\rho F}{Y} \frac{\ell^4}{D'^2} \frac{\left(1 + \frac{4}{3} R\right)}{f} \left[1 + \frac{f}{f_1} - \left(1 + \frac{f}{\ell}\right)\left(1 - \frac{f_1}{\ell}\right)\left(1 + \frac{R}{6 + 8R}\right)\right] \tag{12}$$

wher ρ/Y is the ratio of density to Young's modulus for the structural material, f the focal length and ℓ the physical length of the telescope, f_1 the focal length of the primary mirror, D' the effective physical diameter (about 30% greater than the optical aperture D) and R the ratio $D't_1/2\ell t_2$, where t_1 is the wall thickness of the telescope tube and t_2 the mean thickness of the corrector plate and attachments. Notice that the error for a telescope of given f, f_1 and ℓ is independent of the ratio of focal lengths f_1, f_2 for the secondary and tertiary mirrors. Also that the error for a long focal length system (f/ℓ large) scales effectively as the cube of its physical length. Inserting numerical values, one finds that the image motion on earth is $\pm$ 0.13 arc-second. In space, where the maximum acceleration is about 10^{-6}g, the error is roughly 10^{-7} arc-second,

well within the requirement for the experiment.

The only effective way of reducing the image displacement on earth lies in counterbalancing the gravitational acceleration by magnetic or mechanical forcers acting on the body of the telescope. They would have to be separate and distinct from the forcers used in pointing the gyro-telescope package.

The influence of mechanical creep on the zero stability of the telescope may be taken into account by a modification of equation (12). Two major viscoelastic effects are known to occur in all glasses including fused silica: irreversible viscous motion, which may be described on the Maxwell model by a viscosity η and a relaxation time $\tau = \eta/Y$; and the delayed elastic effect. The latter is a reversible effect which results in a finite extension analogous to the ordinary instantaneous extension but is distinguished from the instantaneous elastic effect by being acquired or lost over an extended time. To a first approximation it obeys the empirical Michelson equation

$$\frac{D_M}{D_Y} = \zeta \left(1 - \exp - \sqrt{t/\tau'}\right) \qquad (13)$$

where D_M/D_Y is the ratio of delayed to instantaneous deflexions and τ' is a retardation time which must be distinguished from the Maxwellian time τ . The creep errors in the telescope may be found by applying the similarity principle of Trouton, which states that creep effects scale according to dimensionally similar formulae to the static elastic

deflexion. Consider now a space telescope. Assume that before the satellite is launched, it is oriented with the telescope axis at an angle ψ from the vertical for a time long compared to τ', so that the delayed elastic deflexion reaches its limiting value ζD_Y. Then the variation of the null point of the telescope in space due to creep effects will obey the equation

$$\theta_c = \theta'_Y \left\{ \frac{Y}{\eta} \frac{F}{g} \tau + \zeta \left(1 - \exp - \sqrt{\epsilon/\tau'}\right) \sin \psi \right\} \qquad (14)$$

where θ'_Y is the maximum elastic deflexion under 1-g load; and Y, η, ζ and τ' are all functions of temperatures, η, and τ' being functions also of the previous thermal history of the material.

For all glasses including fused silica an equilibrium viscosity η_e exists at any temperature, represented tolerably well by the Andrade equation

$$\eta_e = \eta_o \exp - E/RT \qquad (15)$$

where η_o and E are constants. On raising the temperature η is at first larger and on lowering thetemperature it is smaller than the value in equation (14); but if the material is left at another temperature for a sufficient time η gradually approaches the equilibrium value. A glass which is in equilibrium is said to be stabilized; the instantaneous temperature of equilibrium is known as the fictive temperature.

Experiments by Hetherington et al[1] give stabilization times in a typical fused silica of 24 hours at 1200°C, 170 hours at 1100°C and in excess of a year for fictive temperatures below 930°C . Since the viscosities extrapolated to $0^{\circ}K$ from measured data are about 10^{19} poise for a fictive temperature of 1100°C and 3×10^{21} poise for 1000°C , substantial improvement is obtained by stabilizing the material initially at the lowest practicable temperature, i.e. about 1000°C . Inserting $\eta = 3 \times 10^{21}$ poise, $Y = 8 \times 10^{11}$ dynes/cm^2 and $t = 3 \times 10^{7}$ sec (1 year) into equation (13), the zero shift due to viscous creep is $10^{-2}\ \theta'_{Y}$. In space this leads to a completely negligible error, and even on earth the effect on a telescope mounted horizontally for a year is only 0.001 arc-sec.

Information on the delayed elastic effect, although less complete, is sufficient to show that its effects also may with care be made negligible. Measurements by Murgatroyd and Sykes[2] give η 0.0012 and τ' 10^{6} seconds (ten days) for fused silica at room temperature. Hence the zero error due to effects at room temperature cannot exceed $0.0012\ \theta_g$ or 10^{-4} arc-seconds. The most serious question concerns the variation of ζ and τ' with temperature. Experiments on a soda-lime-silica glass by G. O. Jones[3] appear to indicate values of ζ ranging from 0.035 at 200°C to 0.63 at 537°C (the transformation point for the sample). No precise data on the variation of τ' is available, but there is no reasonable doubt that it increases as the temperature is reduced, and for fused silica at 2 K the time τ' must be many years. Suppose the fused silica from which the telescope is constructed

acquires some delayed elastic strain under its own weight while cooling initially from the annealing temperature. The very slow release of the strain at 2 K during the course of the year, might then cause significant null shifts. To eliminate such errors, two precautions appear desirable: (1) the telescope tube should be mounted in a vertical position during the cooling to room temperature (2) after construction it should be left in the vertical position at or a little above room temperature for a substantial period to allow delayed elastic effects to relax before cooling to $4^{\circ}K$. Assuming the validity of the square root relationship in the Michelson equation, the residual effect should be reduced by a factor of ten in time $10\,\tau'$, i.e. about 4 months at room temperature.

The effect of thermal expansion under temperature gradients is calculated in a similar way. Again the null shift is affected by both changes in angle between the mirrors and displacements of the secondary mirror and image divider. Since the angular distortion of an element $d\underline{\ell}$ of coefficient of expansion α is given by $d\theta = \alpha\, d\underline{\ell} \wedge \text{grad } T$, only transverse temperature gradients affect the null point. It is possible to reduce these by surrounding the telescope tube by a sheath of copper or other high conductivity material. The final result is best expressed in terms of the total transverse heat load Q , which for simplicity may be assumed uniformly distributed over the projected area of the telescope. Let the conductivities of the telescope tube and sheath be k and k' and their wall thickness w and w' . The null shift due to temperature gradients becomes

$$\theta_T = \frac{\pi}{4} \quad \frac{\alpha Q}{kw + k'w'} \quad \frac{f_1}{\ell} \left[\left(1 + \frac{\ell}{f} \right) + \frac{\ell}{f} \left(\frac{f}{f_1} - 1 \right) \right] \sin \phi \qquad (16)$$

where ϕ is the angle between the heat flow and the plane of the image divider.

Equation (16) may be transposed into an expression for the maximum allowable heat input Q_{max} into the telescope. Inserting numerical values for α and k, taking the wall thickness of the telescope and copper sheath as 1 cm, the following results are obtained

Table I

Maximum Allowable Heat Inputs (mW)

	2 K	77 K	300 K
without copper sheath	3 mW	0.002 mW	0.01 mW
with copper sheath	5×10^3 mW	0.1 mW	3 mW

The heat load due to direct solar radiation falling directly on to a telescope covered on the outer surface with a second surface mirror is about 1000 mW or about 500 times the maximum allowed at room temperature, even with a copper sheath. In such circumstances the null shifts would be about ± 0.5 are second. The error could be reduced by perhaps a further factor of 50 by the use of superinsulation

but would then still be 10 times the specified maximum. On the other hand at cryogenic temperatures the total heat input into the helium dewar is about 75 mW , or about 1% of the maximum allowed.

Thus the low temperature environment is essential to making a telescope of the required precision. It should be noticed that relatively little is gained by operating at the temperature of liquid nitrogen (77K).

The position of the focal plane of the telescope changes slightly on cooling from room temperature to liquid helium temperatures. The existence of the effect was first shown by R. Woodruff of Ball Brothers Research Corporation. It causes an image shift ∂ along the axis of

$$\partial = \bar{\alpha}\, \ell \left(\frac{2f_2f_1 + 3f_1\ell - 3\ell^2 - 6f_2\ell}{f_2f_1 + f_1\ell - \ell^2 - 2f_2\ell} \right) \left(T - T_o \right) \quad (17)$$

where $\bar{\alpha}$ is the mean coefficient of expansion between T and T_o . The net shift is about 50×10^{-3} inches. The change in image diameter is negligible.

2.3 Conclusion

The foregoing equations give a basis for the design of a high precision star-tracker. They show that the desired performance may be reached by exploiting the combination of space and cryogenic techniques. However to do so several other sources of error have to be eliminated for example, the effects of differential changes in the transmissiblity of the light-pipes, error in the chopping wheel and detector, the effects of stray light. Many of these are covered in sections 3 and 4

below. One important conclusion based partly on the analysis and partly on the experiments with the simulator described in section 4, is that it is best not to defocus the image. The advantages of working with a diffraction limited image are three

(a) the photon noise is a minimum

(b) all null shifts due to differential changes in the detection channels(such as aging of the light pipes, or the combination of aging of the photocell with imperfect superposition of the matched signals) scale linearly with image diameter d . Hence they are a minimum with diffraction limited optics.

(c) With defocussed optics the image is essentially a pinhole view of the telescope aperture. Thus any uneven darkening of the aperture or mirrors during the year causes a null shift.. With diffraction limited optics that error is almost completely eliminated since each point on the image is illuminated by light from the entire aperture.

The difficulties in working with a telescope with diffraction limited optics are: tighter requirements on telescope pointing (equation 4) and on the size of chips on the roof prisms (equation) and the general need for better quality optics. However all of the requirements can be met. An interesting feature of the diffraction limited system, is that its noise performance scales as the square of the aperture (equation 9) rather than linearly. This is because the image diameter decreases at the same time as the number of photons increases. Hence the improvements gained through increasing the aperture may be considerable. There is, of course, a limit to the size of a

telescope for which it is feasible to make diffraction limited optics.

It should be observed that all the calculations given here have been for an ideal isolated star. In fact Rigel has a companion situated about 9.4 arc-seconds away, whose brightness is 1/400 of the main star. The effect is to throw extra light into one side of each readout channel causing null shifts of ± 0.0013 arc-seconds, which change sign as the satellite rolls through 180° . The error can be taken out precisely in data analysis. There would be trouble if the secondary were more nearly equal in brightness, because the image could eventually be displaced into its non linear region. In fact with two sources of equal brightness, separated by angular distances greater than the image diameter, the star tracker would cease to work.

3. DESIGN AND ASSEMBLY OF TELESCOPE OPTICS

3.1 Design Features

The general optical design has been described in section 1. This section gives a few fruther details. The two main parameters of the telescope are its aperture D and focal length f . The choice of a 5 1/2 inch aperture was dictated by photon-noise performance, allowing for losses in the optics and detection system. Actually a slightly smaller aperture could be accepted in the final flight experiment, but there is little point in doing so since there are other reasons for having a 9 inch neck-tube in the dewar, based on the requirements for the gyro spin up system, and therefore a telescope of this aperture fits in nicely. The focal length has to be long enough

to reduce errors due to nicks on the dividing edge (equation 10) On the other hand with a given physical length there is an upper limit to the focal length that can be attained without degrading the image quality. The present physical length of the telescope (13 inches) was about as long as seemed convenient, and with that the 150 inch focal length was taken as the maximum practicable value. These parameters were fixed before the method of making the roof prisms had been perfected. Actually the prisms turned out better than was expected, so the nick criterion was more than met. In retrospect there might have been advantages in having a slightly longer physical length (say 14 to 15 inches) and a slightly shorter focal length (say 120 inches).

The telescope consists of the following parts, all of which except 16 and 17 are shown in figure 1.

1. Primary Mirror (spherical concave)
2. Secondary (spherical convex)
3. Third mirror (spherical convex)
4. Corrector Plate (aspheric)
5. Support Tube
6. Cover
7. Box
8. Relay Lines
9. Roof Dividers (2)
10. Beam Splitter
11. Support for Item 10
12. Deflector Mirrors (2)
13. Deflector Mirrors (2)
14. Base
15. Gyro Mounting Ring
16. Light Pipe Guide
17. Wire Clip
18. Light Pipe

Design and manufacture of most parts followed established optical prccedures, adapted in some places to make the structure suitable for assembly by the optical contacting technique. The following special

points may be noted:

(a) Since the telescope is made to operate in an evacuated chamber, pump out holes are provided in the support tube and light box. These are located where they may also be used in cleaning the optics and in attaching extra light baffles, without taking the contacted joints apart.

(b) The roof prisms were made and checked in the following way. First two rough cubes of quartz (about one inch side) were polished flat on one face and optically contacted together, with provision for separating them afterwards. Then a second polished cut was taken across the two joined blocks, accurately at right angles to the first. In this way two rooves were formed, with the prisms protecting each other's edge against damage. The parts were separated and checked for nicks at NASA Marshall Center, using first the Cambridge Scanning Electron Microscope, and then a simpler optical technique, developed by Mr. W. Angele, which could be reproduced at Davidson's to watch the prism edge during assembly. This technique consisted essentially in illuminating the prism edge obliquely and looking for the diffraction haloes of light scattered from nicks.

(c) The beam splitter constituted a difficult part of the design. Conventional beam splitters are made from two cemented 45° prisms with a half-silvered interface. The decision to avoid cements precluded an arrangement of this kind; so instead a half-silvered plate tilted at 45° was used. As a result there was some astigmatism in in the transmitted star image, but trouble was avoided by using that

image for the readout axis in which the astigmatism was parallel to the roof-line.

(d) To help in assembly four light pipe guides with spring clips were contacted to the corrector plate where the light-beams leave the deflexion mirrors, so that the pipes could be attached in position after the telescope has been mounted on the dewar.

3.2 Assembly and Alignment Procedure

The following account of the assembly procedure has been supplied by Mr. D. E. Davidson. Reference should be made to figure 1 where necessary.

1. The primary mirror was contacted to the base in a mechanically centered position.

2. The tertiary mirror was contacted onto the base mechanically centered in the hole in the primary. An aluminum wedge shaped sleeve was used in centering as the mirror was pressed into contact.

3. The tube was next contacted onto the base mechanically centered (by eye).

4. The secondary was contacted onto the flat (uncorrected) side of the corrector plate.

4.1 The center holes provided the reference for centering.

5. The corrector plate (with secondary attached) was now contacted onto the tube.

5.1 To assure proper alignment, three 1 × 2 × 4 pyrex blocks were contacted to the bottom surface of the base so that a of each block extended out 1 1/2 inches from the edge of the base.

5.1.2 The base plane and parallel to 1 arc second and thus the bottom reference surface is normal to the optical axis.

5.2 The telescope was placed on a granite flat resting on the three pyrex blocks with the optical axis vertical.

5.3 A Davidson Autocollimator, Model D638 (2 1/2 inch aperture) was then supported above the telescope and sharing aperture with the telescope and one of the block, so that half of the beam was reflected from the block and the other half passed through the telescope and come to a focus just about the corrector plate.

5.4 The beam was aligned normal to the block and then the corrector plate and secondary assembly were positioned so that light from the D638 came out centered in the hole in the corrector plate and contact made to the tube in this position.

6. Beamsplitter

6.1 The beamsplitter (10) was next contacted to the support (11) with the beamsplitting surface down.

6.2 The support and beamsplitter was next contacted to the corrector plate using Method 5.3 to assure proper centering.

7. Focal Position

7.1 The telescope was next laid on Vee Blocks on the corrector plate fixture and using a pinhole and knife edge at the focal plane the telescope was adjusted to autocollimate off a 6 inch diameter optical flat mounted normal to the telescope axis. The observer stood at the side of the telescope and viewed the image through a right angle prism.

7.2 The position of the knife-pinhole assembly was adjusted until a uniform cut-off was seen over the entire aperture and then the distance from the pinhole to the corrector surface was carefully measured. This position is the focal position.

8. Box Height

8.1 The height of roof divider (9) was carefully measured using a measuring microscope so as not to damage the roof edge.

8.2 The box was then made the exact height to bring the roof to the focal point.

9. First Roof Divider

9.1 This divider is the one attached to the corrector plate. The same set up was used as in the alignment procedure 5.3, except with a microscope added to view the image of the prism on an enleraged scale.

9.2 With the collimator in perfect alignment, the prism was contacted so that the edge split the star image from the collimator.

9.3 Focus is not as accurately assured in this roof prism position as for the second divider (11 below). As a double check the position was measured directly and it was observed that the microscope image was sharp at the same time as the knife edge was sharp.

10. Box

10.1 The box was next contacted on in such a position that the light from the roof splitters came out through the proper holes in the box.

11. Cover and Second Roof Divider

11.1 The roof divider was contacted onto the cover centered by eye.

11.2 Using the same setup as 9.1 except looking through the appropriate hole in the box, the roof and cover assembly is contacted into place with the roof splitting the star image.

11.3 By moving the collimator while viewing the roof through the microscope, the star image could be made to travel across the roof. After the image was brought to bhe best judgement of cut in half, the error to the reference block was read from the autocollimator. This error appeared to be no more than 1 second of arc. The D638 will repeat to .1 - .2 second arc.

12. Deflector Mirrors (12)

12.1 All four deflector mirrors were next contacted into place by visual positioning.

13. Lenses (8)

13.1 The lenses were next contacted in place such that the image of the star from the collimator fell on approximately the center of the deflector mirrors.

14. Light Pipe Guide (16)

14.1 The light pipe guide was next contacted in such a position that the star image should enter a 1/8" diameter light pipe held in the Vee of the guide.

14.2 After assembly as per above, the telescope was placed in the beam of a large (20" diameter by 120" F.L.) collimator and the star image appeared to come out each light pipe guide properly.

Pictures of the assembled telescope are reproduced in figure 3 and 4.

4. DESIGN AND TESTING OF DETECTION SYSTEM

4.1 Light-Chopper and Detector

The photon noise equations established the feasibility of constructing a telescope to detect 0.001 arc-sec displacements with integration times of a few seconds. To achieve such precision other sources of noise and null drift have to be removed. That requires careful attention to detail in the design of the light choppers and readout system.

The light chopping technique greatly reduces the error due to aging of the sensitive surface as compared with (say) the use of a split photocell. Even so the desired null stability does not come easily. Thus it is known that in space the sensitivity of a typical photomultiplier decays by as much as 60% during the course of a year. Assuming a variation in the aging of 20% over the cathode surface (i.e. that the decay ranges from 54% on one side to 66% on the other) one finds with an image diameter of 0.9 arc-second, that the output beam from the two light pipes A and B in each channel have to overlap on the cathode by 90% or more to be sure that there is no null shift greater than 0.001 arc second.

As was remarked in section 1, the design is much simplified by having completely independent detection systems for the two readout axes. Figure 5 illustrates the design of the chopper. It consists of a 3 inch diameter rotating disc with four slots, two for the readout signals and two to derive timing signals for use in the electronics, obtained by means of small lamps and diode detectors. To eliminate

stray light the photodetector and chopper form a single unit, and there are a series of intersecting light-baffles in the case and the rotating disc. The chopping frequency is 50 Hz. The first design had pairs of f/3 lenses to focus the emergent beam from the light pipes and transmit it to the detector. Heavy light losses resulted. Aftera lot of experimentation the best approach found was to eliminate the lenses entirely and make the distance from light-pipe to photocell as short as possible. With this arrangement the ends of the pipes have to be tilted towards each other to have th output beams superimposed. Figures 6 and 7 show the completed parts.

Ther would be some advantage in taking the timing signals from capacitative measurements on slots milled in the chopping wheel, rather than from the lamps and diode detectors. The wheel would be smaller and would require fewer light baffles. In a space version that should probably be done. The present design was chosen for use in the laboratory because it had already been checked out in the simulator experiments described in section 4.3. Some details of the assembly shown here were determined by the exigencies of the laboratory set-up. A problem that caused difficulty was the magnetic shielding and cooling of the drive motor. When the chopper is run in air viscous drag in the closely intersecting light baffles is surprisingly large. Hence the drive motor has to be more powerful than one might expect (10 watt). Since the motor has also to be surrounded by a good magnetic shield (to minimize its magnetic effects on the gyroscope), it has to be cooled by a forced draft obtained from an external source of air. Care then has to be taken that the air currents do not interfere with the telescope tests. There would be advantages to doing some more development

work in this area.

The most likely sources of random noise inputs into the system other than photon-noise, are the intrinsic voltage fluctuations in the photo-detector and the pre-amplifier. A comparison of calculated noise inputs from various sources, including a variety of possible light detectors is as follows. The figures are evaluated in microvolts at the input of the amplifier, using integration times of 2.5 milliseconds and reduced to comparison with the value obtained for a 20 kΩΩ load resistor on a 1P21 photomultiplier which was the detector used in the original simulator experiments. For the photon noise figure on optical efficiency of 10% and a quantum efficiency in the detector of 12% is assumed.

Table 2

Comparison of Expected Noise Voltages (μV)

photon noise due to starlight	diffraction limited image	30
	20 arc-sec image	400
noise due to photodetectors	selected 1P21 photomultiplier	20
	selected 4441A photomultiplier	15
	phototransistor	7×10^4
	photofet (field effect transistor)	5×10^4
noise due to transistor in readout preamplifier circuit		0.3

The table shows that phototransistors and photofets generate excessive noise, and cannot be used to approach the photon noise limits. On the other hand, either photomultiplier used in conjunction with the transistor amplifier is acceptable. The present detection system uses 4441A photomultipliers, specially selected for high sensitivity and initially matched to 10% in the two channels. The 4441A has a lower inherent gain than the 1P21 but has two advantages. Its quantum efficiency is higher (15% as compared with 12% for the 1P21); and its configuration being end up rather than sideways on, allows the photocathode to be put nearer to the ends of the light-pipes reducing the optical losses. It should be said that some of the newer solid state light detectors, which were not available when the design was made, have better performance than those shown in the table, but still do not reach the photon noise limit.

4.2 Readout Circuitry

The preamplifier designed by R. A. Van Patten of Stanford Aeronautics and Astronautics Department is illustrated in the schematic diagram of figure 8. The circuit employs a monolithic integrated differential amplifier, with a field effect transistor operating on a variable feedback shunt to provide gain control capability.. Experimental versions have been built up and tested extensively - both on the bench and with the simulator - and been found to give satisfactory performance over a gain control range of 25 to 100 volts/volt.

In preliminary experiments with the simulator a serious zero error was observed, arising from asymmetry in the shapes of the transition

regions between the 0° and 180° signal levels derived from the light-chopper. The magnitude error varied with both the amplifier gain and the position of the star image. Two steps were taken to remove it. The ends of the slots in the chopping wheel were carefully shaped to minimize the spikes in the photomultiplier output arising in periods of overlap or underlap. The circuit was equipped with a MOSFET series shunt chopper and buffer amplifier to blank out the signal in a small time range around each transition. The use of a chopper giving smooth transitions is necessary even though the amplifier itself operates continuously and is subject to overload disturbances, which might persist long enough to cause error, if significant spikes do occur. Time symmetry of the signal is guaranteed by using a common integrated circuit single-shot multivibrator to blank out both transition regions. Two quadrupole gates and two additional integrated single shots complete the timing logic. A d.c. restoration filter guarantees the voltage symmetry of the signal. The d.c. bias present at the photomultiplier output is removed by taking advantage of the capability of the integrated differential amplifier to reject common mode signals. Voltage limiting is privided at the input to protect against excess voltages due to exeessively high light levels.

The linearity and noise data reported in section 4.3 below were obtained using this amplifier near maximum gain in combination with a North Atlantic phase angle voltmeter operating usually at its most sensitive range of 1 V rms full scale. The 50 cycle/sec reference square wave derived from the light chopper was used directly by the

preamplifier but was filtered to a sine wave before application to the phase angle voltmeter. The voltmeter requires sine wave reference but accepts the chopped waveform as a signal input.

4.3 Preliminary Experiments with the Telescope Simulator

A model telescope and artificial star were set up at Davidson's in 1966 on an iron beam about [illegible] feet long and 5 inch square channel section. The original arrangement was symmetrical, both telescope and collimator being parts of standard Davidson autocollimator of 20 inch focal length and 2 1/2 inch aperture. Afterwards the focal length of the collimator was increased to 60 inches to reduce the geometrical image wire. The illumination for the artificial star was derived from a 6 volt bulb, the intensity being varied by adjusting the lamp voltage. It was transmitted through a pinhole, of which two of different diameter have been used: a 4 mil hole corresponding in the original set up to a diameter of the in-focus geometric image of 40 arc-seconds and an 0.5 mil hole corresponding to a geometric image of 5 arc-seconds. Taking diffraction into account to effective diameter for the 0.5 mil holw was about 6.5 arc-sec. With the 60 inch focal length, the 0.5 mil pinhole yeilded a geometric image of 1.7 arc-seconds, which meant that the diameter of the final image was essentially determined by the diffraction limit, in this case 2.2 arc-seconds. Defocussing was effected by moving the detector. A displacement of 23 mils from the focus gave a 20 arc-second diameter image, with the 25 inch focal length used. A tipping plate was put in the diverging beam of the artificial star, by means of which the image could be displaced over a range of ± 6 arc-seconds in the horizontal plane. The dial was

was calibrated in units of 0.01 arc-seconds. Great care was taken to eliminate stray light from the entire system, by having a hood over the gap between the star and telescope objectives, and by working in a darkened room.

The system was calibrated directly against real stars by means of a stellear photometer, made from another telescope of 20 inch focal length and 2 21/2 inch aperture. For night sky observation the photometer was mounted on a portable clock drive. A beam splitter allowed a star to be selected from the field by eye and simultaneously measured on a 1P21 photomultiplier or other attached detector. A stop in the image plane delimited the field to a strip about 10 arc-sec wide and 200 arc-sec long. A computation based on known losses in the optics indicated that about 16% of the light entering the aperture reached the photomultiplier; the major part of the loss being due to the beam splitter. The original photometer was the property of Davidsons's. Another slightly improved design has been made under the present Contract and delivered to Stanford.

Night sky observations were carried out at West Covina on January 18, 19, 1967. The photomultiplier employed at that time (a 1P21) was operated in conjunction with a 666 kΩ load resistor and the output voltage was measured with an oscilloscope. The observations were used to calibrate the artificial star by attaching the photo-meter to the collimator to read its output directly. Different star signals were simulated by adjusting the lamp voltage. The left hand ordinate

on figure 9 gives the measured output of the photometer photomultiplier with a 666 kΩ load resistor. The two curves show the variations of intensity with lamp voltage for 4 mil and 0.5 mil pinholes mounted in the 20 inch collimator. A further curve(not shown)was afterwards calculated for the 60 inch collimator. Points derived from the manufacturers rating of the lamp, fitted arbitrarily at one point to the curve for the 0.5 pinhole, show reasonable agreement with themeasured results. The horizontal lines on figure 9 give anticipated intensities of Procyon, Rigel and Polaris, with a numberical correction such that the intensity corresponds to that entering each channel of a two-axis telescope of 5 1/2 inch aperture rather than the single axis 2 1/2 inch telescope actually used. There was some discrepancy between the observed intensities and these computed from known stellar magnitudes, using the known optical loss in the photometer and the photomultiplier rating. The disagreement was attributed at the time to atmospheric losses in the murky air of Southern California. However that may not be the right explanation. We intend as soon as possible to re-calibrate the entire system with the improved photometers.

The right hand ordinate of figure 9 gives results of light level measurements with the telescope and the original version of the chopper detector in place of the stellar photometer. They were obtained by directing all the light down one of the light pipes, running the telescope photomultiplier at the same voltage as that on the photometer, and correcting to the same load resistor of 666 kΩ . The numerical ratio of the two ordinates shows that the optical efficiency of the system was 2.8% of that of the photometer. Since the photometer

efficiency was known to be 16%, the conclusion is that only 0.4% of the light entering the telescope reached the detector. This result was intensely disappointing. It was confirmed in another way be mounting the photomultiplier of the focal plane of the telescope using an adapter ring in place of the chopper-detector assembly. Measurements on the light pipes by themselves disclosed that the losses there were only 10 to 20% over the one foot length. Eventually it became obvious that almost all the loss took place where the light left the light-pipes and entered the chopper-detector assembly. Several tests made it clear that the only hope for improvements was to shorten the distance between the light pipes and the photomultiplier, and that accordingly was done in the detector for the present telescope.

Measurements were made of the noise equivalent angle versus star intensity. Figure 10 gives a comparison of the experimental results with the theoretical photon noise calculated from equation (8) for 6.5 arc-second and 30 arc-second images formed by a telescope with no central obscuration. The experimental points were estimated visually by watching the magnitude of fluctuations of the readings on the North Atlantic phase angle voltmeter over periods of about 30 seconds. The bandwidth of the meter is about 3 radians/sec. The agreement between visual estimates repeated blind was within about 10%. The theoretical curves were derived using an optical efficiency of 0.45% as measured and a quantum efficiency of 12%, taking the bandwidth $\bar{\nu}$ as 3 radians/sec. Also shown is the theoretical curve for a diffraction limited image (in the 2 1/2 telescope) determined from equation (9). Since the

star intensity was varied by varying the lamp voltage, a correction for changes in the color temperature of the lamp had to be applied. Without correction $\bar{\delta}_v$ varies as $I^{-0.5}$. Reference to equation (8) and (9) show that changes in temperature cause an increase in exponent for a diffraction limit image and a decrease in exponent for a defocussed image. Estimates of color change were made by eye and the curves corrected accordingly. The agreement between observation and theory is good, perhaps flukishly so considering the approximations made. The residual noise from the photomultiplier with the star lamp extinguished was about 10% of the observed noise in the 6.5 arc-sec image of Procyon. The noise due to the transistor amplifier alone was negligible.

Linearity measurements are presented in figures 11 and 12. In obtaining the readings care was required to avoid false results due to zero drift of the simulator. Even under quiet conditions there were zero motions of as much as 1 arc-sec in periods of a few minutes. Zero checks were therefore made between each measurement, and for the more precise observations the results were checked three times. The experiments brought home to us, as calculations never could, the realities of small fractions of a second of arc. They fully confirmed the statements made in section 3.2 about the difficulty of stabilizing an optical system at room temperature. The two figures give data for the central portions of 6.5 arc-second and 30 arc-second images, with positive and negative halves superimposed for comparison. As anti-

cipated, defocussing improved linearity but decreased sensitivity. The asymmetries in the curves shows that the non-linearities in this particular system are not represented by the term $2s^2/3d^2$ in equation (2). Microscopic examination of the image and study of the complete curve (not reproduced) gave some grounds for attributing the nonlinearities to unequal transmission in the two halves of the detection system rather than aberrations in the telescope itself. Thus we must be on the lookout for similar effects even with the higher quality optics of the actual star-trackers. Although the non-linearities do not have the symmetrical form of eq. (2), the following comparison is of some interest:

Table 3

Comparison of Theoretical and Experimental Linearity Data

	6.5 arc-sec	30 arc-sec
predicted range 1% deviation	± 0.4	± 1.7
observed range (deviation exceeding experimental error)	± 0.4	± 1.2

Measurements were made of the effects of introducing disc and barrel shaped obscurations in the aperture for the defocussed telescope.

They made things worse rather than better. However since the non-linearities were of opposite signs in the two cases it seems likely that some other form of obstacle accuratley shaped and placed, might help. Practical difficulties made the experiment not worth pursuing on the simulator.

4.4 Measurements on the New Chopper-Detector

Much work remains to be done in evaluating the new chopper-detector. However the preliminary results are encouraging. The simulator was set up at Stanford and data taken on May 1972. The measured optical efficiency was in the range 5% to 20%, which compares very favourably with the figure of 0.45% for the original assembly. For some reason not yet understood the efficiency vaired with focal position. Measurements were also begun on noise performance. However so many changes have been made in the simulator as well as the detector that a complete recalibration will have to be made before reliable data can be had. To prepare for further experiments we ordered the new stellar photometer and a small microscope for use in studying the images by eye. These devices have now been delivered to Stanford.

5. EXPERIMENTS ON OPTICAL CONTACTING

Following the receipt of NASA Report CR-61385 on optical contacting Mr. D. E. Davidson performed some experiments under the present Contract to evaluate the technique more thoroughly. The Report had contained an analysis of the process based on the theory of van der Waal's forces, together with some account of experiments done in NASA Marshall Center with contacts on 1/4 wave surfaces. One of the NASA results was the

discovery that contacted surfaces may come apart when soaked in penetrating oil. The following is extracted from a letter of D. E. Davidson to C. W. F. Everitt dated 24 May, 1972.

> "First I contacted two pieces of fused silica (1 3/8" diameter by 1" long) together. These pieces were flat to better than 1/20 wave. They were so tightly adhered I could not wring them apart. Within an hour of contacting them, I soaked them in penetrating oil and left them over night e.g. about 15 hours. After this period of time the contact joint had been penetrated by the oil and they were easily slid apart.
>
> Next parts were cleaned and again contacted together. They were then put in an oven at 250° from Friday evening to Monday morning -66 hours. The contacted pieces were then soaked in penetrating oil for 24 hours. This time the oil did not penetrate the joint and the parts were apparently firmly contacted. It was impossible to pull or twist them apart by hand.
>
> I believe it takes some time for the air and water to get out of the joint.
>
> We make and sell items by contacting optical surfaces and they do not separate in time. We have some pyrex parts that have been contacted for nearly twenty years now and they are still tightly contacted. Fused silica is better for contacting than pyrex - I belive this is because it has a lower thermal coefficient.
>
> We had some 1 3/4 × 3 pieces of pyrex that had been contacted to a large 12" diameter by 2" thick optical flat. This assembly laid in the shop for about 10 - 12 months and then we decided to take it apart. The parts were so tighlty adhered that it took days to remove them even though they were pyrex. We used all the thermal shock we dared and still not break the large disc. The pieces were finally removed by driving steel wedges into the chamfer with a hammer. Pieces of glass were broken from the surfaces.
>
> We have found that parts that have been contacted and then put in a vacuum tank for coating are tighter than before.
>
> Regarding water and moisture, on a humid day, parts seem to contact somewhat easier but there is a likelihood of what we call "false contact." This is a contact joint that is invisible as it should be but which can be twisted by hand - sometime only a second of arc - but still can be moved by heavy pressure. I think that moisture makes "contacting" "easier" for two reasons.

First, dust is not so attracted to the surfaces and second, the parts are not really in contact. On humid and rainy days, we do not like to do contacting.

The next problem is dust. The skill of the contactor is involved here. It is readily possible to do good contacting in the environment of an ordianyr optical shop. Proper lighting is very helpful so the operator can see the closeness of the surfaces. One thing further, parts that have been brought close together and did not go into contact very often get minute gouges and scratches on them that can hardly be seen that seem to have ridges next to them that hold the surfaces apart. These must be removed before a good contact can be accomplished.

To summarize:

1. I am sure that a good contact will not come apart with time.

2. Contact joints get stronger as they get older.

3. Contact joints are stronger after being in a vacuum.

4. Contact joints are very much strengthened by prolonged heating.

If we make a contacted telescope for orbiting service I suggest it be baked for a couple of weeks at about 300°F . I think this would make the joints very strong. I would like to continue experiments on contacting but I have the confidence our telescope will stay together. The only joints that are at all unusual to me are those on the tubes. This is because the tube is somewhat porous. However, I do know that tubes like these are used to make lasers and there has been no real problem with the end mirrors contacted on the ends."

Some work has been done at Stanford on the behaviour of contacted joints at liquid hleium temperature. In experiments with quartz parts performed about five years ago the joints held successfully under repeated cycling, even when the specimen (about 3 inch × 1 inch) was dunked direclty from room temperature into the helium. Another

remarkable experiment was the following: - A 2 inch × 2 inch × 1 inch box was made from two 1/2 inch thick quartz pieces, contacted together in one of which there was a small chamber and a 3° conical taper hole. A coned quartz pipe was epoxied into the hole and connected to a helium leak detector. The box was then placed in liquid helium. No detectable leak was found even when the helium was in the superfluid.state. These early results were highly encouraging. One disturbing experience more recently was when a crown glass contacted joint came apart at liquid nitrogen temperatures. This apparently is a well-known phenomenon in the trade. Some experiments with new quartz pieces confirmed the earlier conclusions that quartz is reliable under temperature cycling.

We agree with Mr. Davidson that more experiments should be tried on the contacting technique.

6. FURTHER TEST PLANS

As was said in the Introduction, testing of the telescope is a long and difficult process. We foresee a series of experiments which will test at least a year, and even then there will be anumber of unanswered questions. Some of the tests to be made will entail reference from the telescope to the gyroscope in the fully assembled laboratory apparatus. An important element in the test program is a new precision Artificial Star, now under design by D. E. Davidson, which we expect to have delivered to Stanford by January 1973. This device has 400 inch focal lenght, 8 inch optical aperture, with an off-axis parabola as the primary mirror. It stands vertically in an eight foot high tube, and has an auxiliary plane mirror to reflect light into the telescope, which may be mounted horizontally or inclined with the dewar and gyro package

at 37° from the horizontal (i.e. true norht at Stanford lattitide). The following outlines a few of the proposed tests.

(a) More detailed evaluation of the chopper-detector systems with the existing telescope simulator, along the lines of the preliminary experiments described in section 4.3

(b) Direct noise performance measurements on the actual telescope using the new Davidson Artificial Star, calibrated against the night sky by means of the stellar photometer.

(c) Studies of telescope linearity. Owing to drift in the test equipment the measurements have to be done dynamically by means of an automatic tipping plate in the Artificial Star. The drive frequency must be neither too high nor too low, being bounded by the chopping frequency of the telescope readout and the bandwidth of the painting servos (which can however be reduced for the test).

(d) A cross-check on the calibration for (c) is obtained by making the telescope follow the star image and observing the motions in the gyro readout.

(e) Creep Tests. These can be done by comparison of the long term image motion with autocollimator measurements to subsidiary reflecting surface on the front end and base of the telescope.

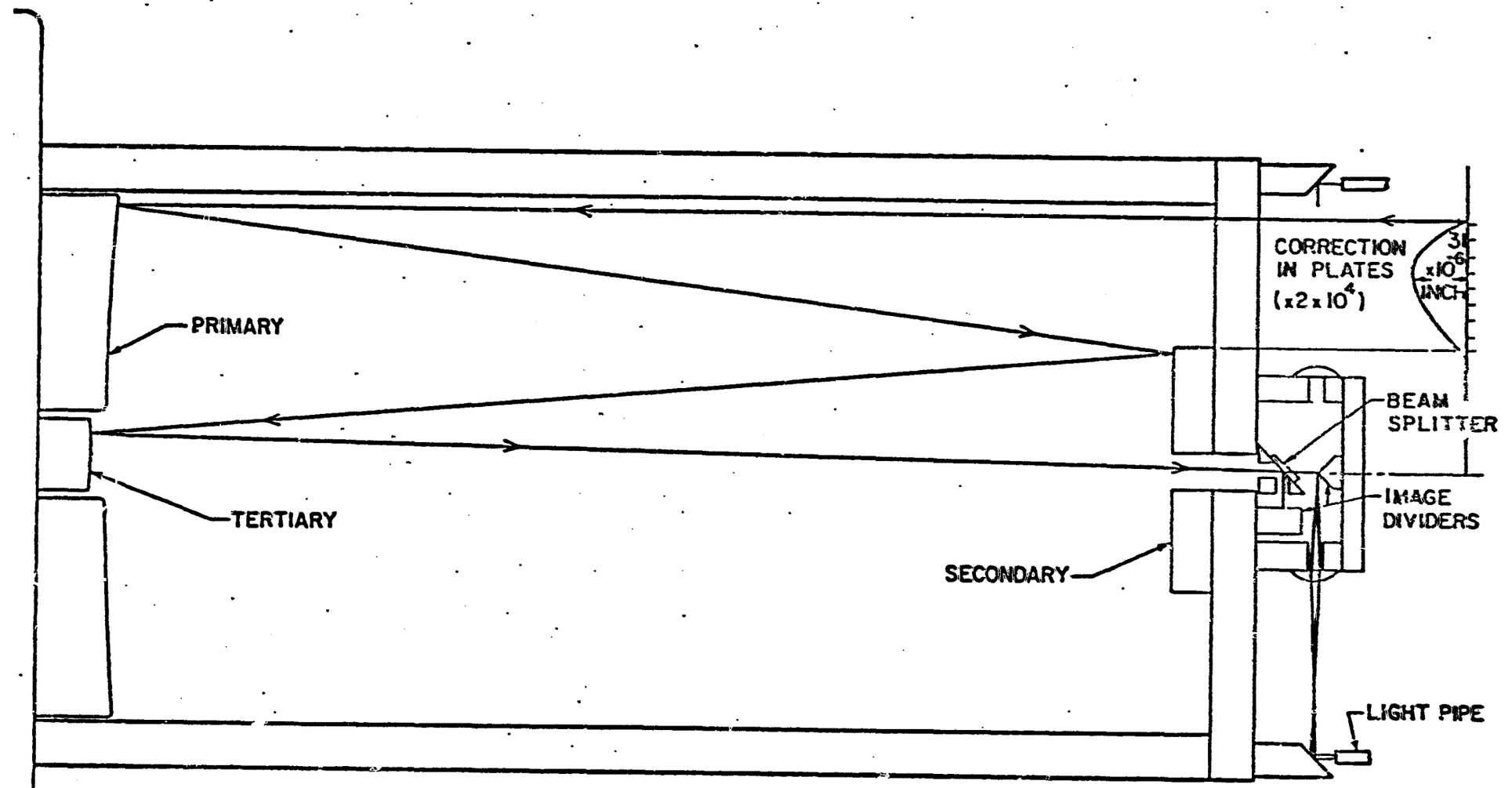

EFFECTIVE FOCAL LENGTH : 150 in. APERTURE : 5.6 in.
PHYSICAL LENGTH : 13 in.
RADIUS - PRIMARY : 46 in.
RADIUS-SECONDARY : 70.050 in.
RADIUS-TERTIARY : 7.9517 in.

Fig. 1 General View of Telescope

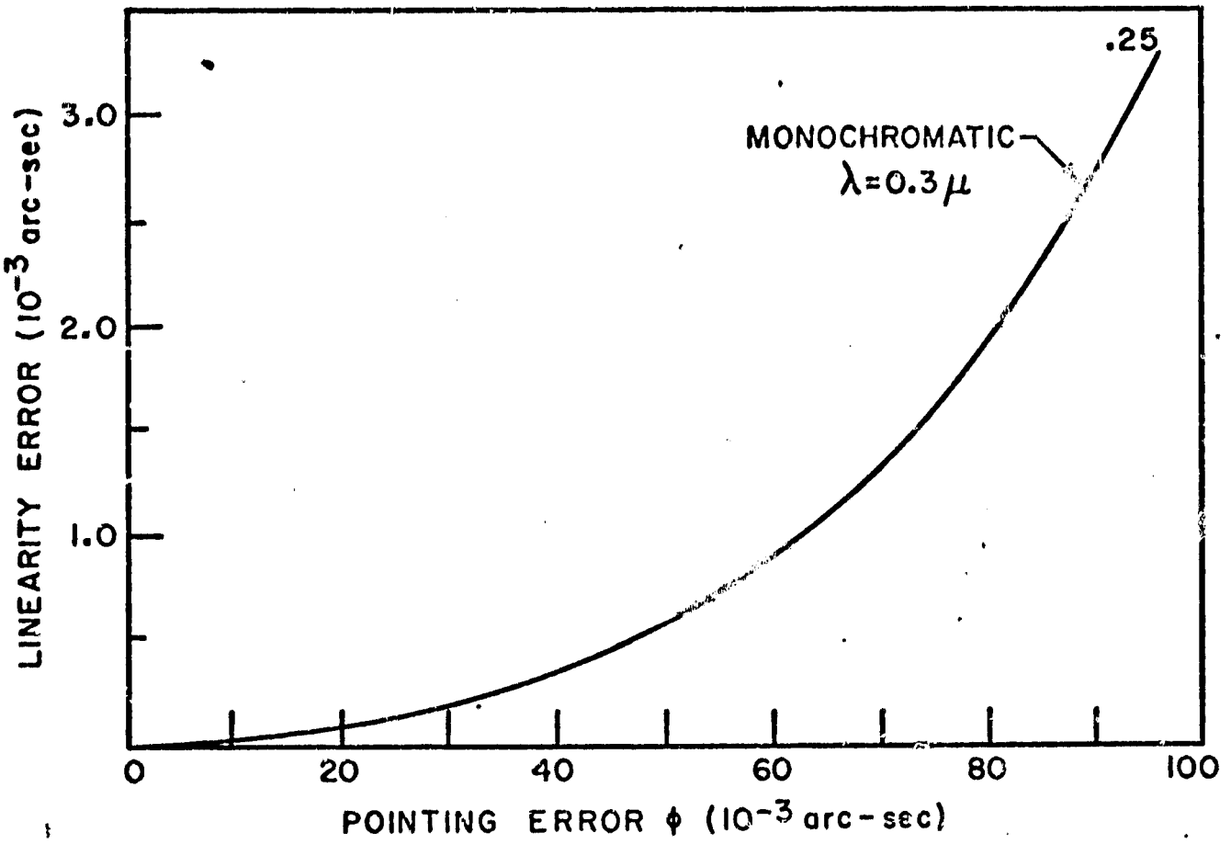

Figure 2 Telescope Linearity

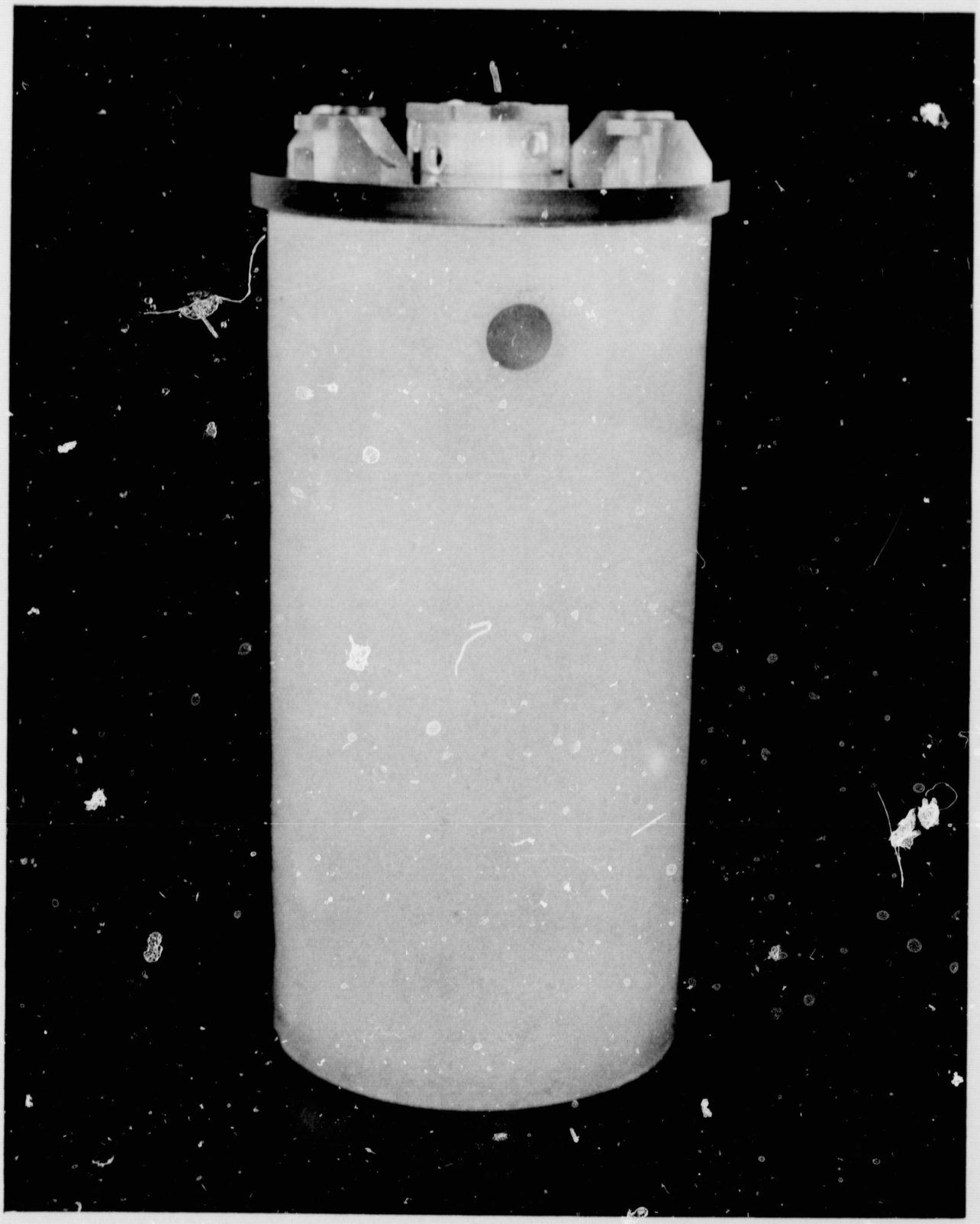

Figure 3 General View of Telescope

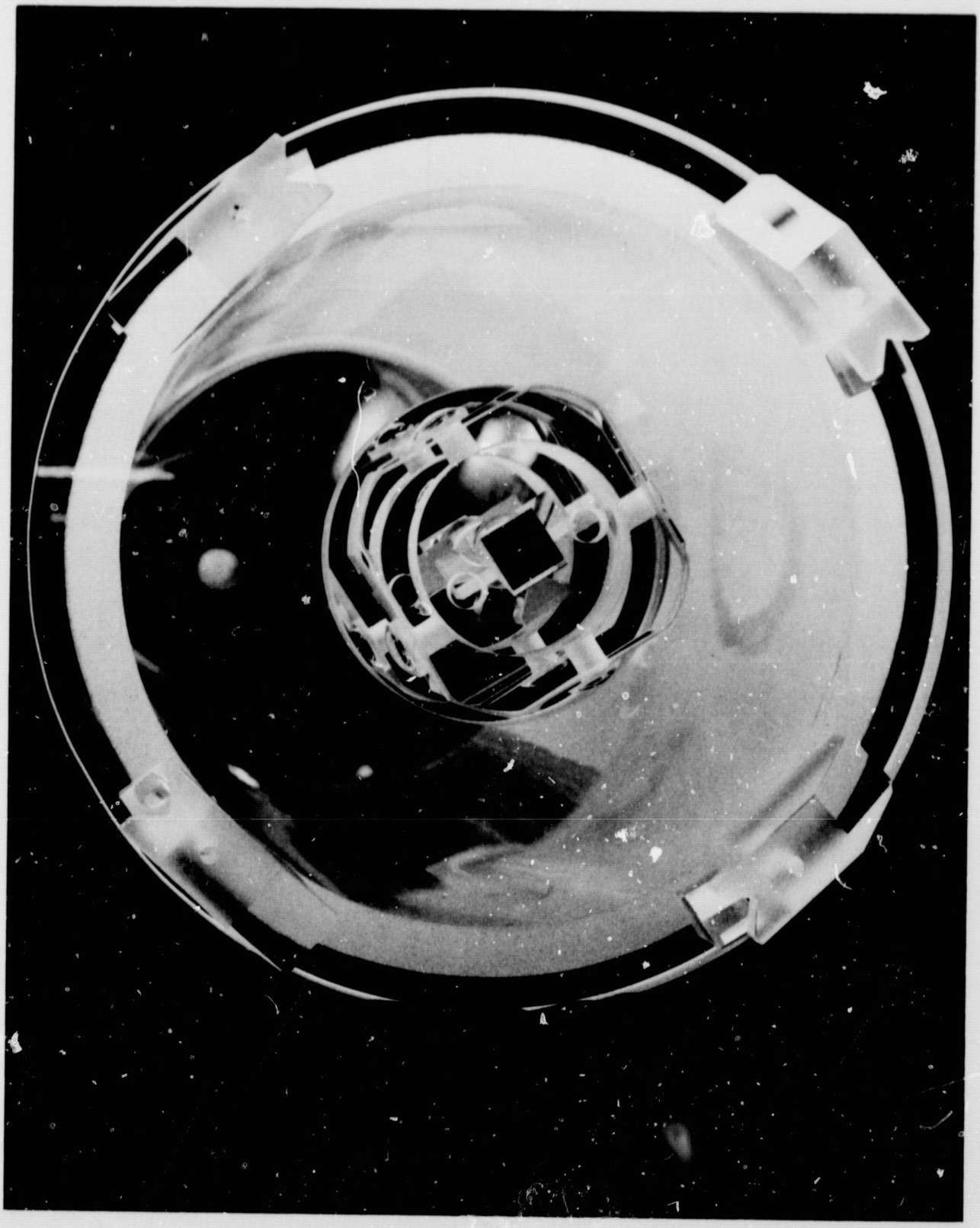

Figure 4 Light Box and Corrector Plate

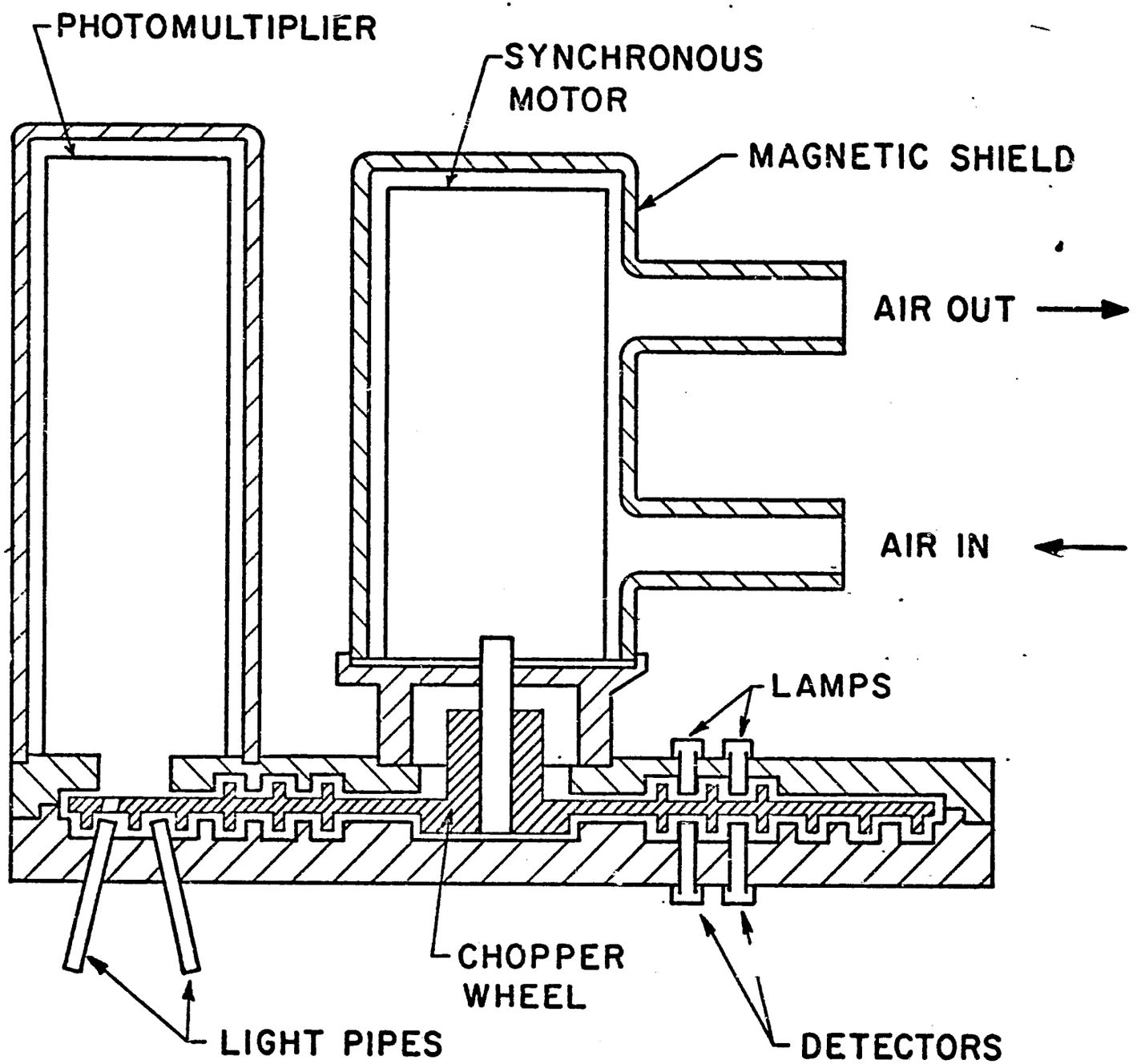

Figure 5 Design of Light-Chopper and Detector

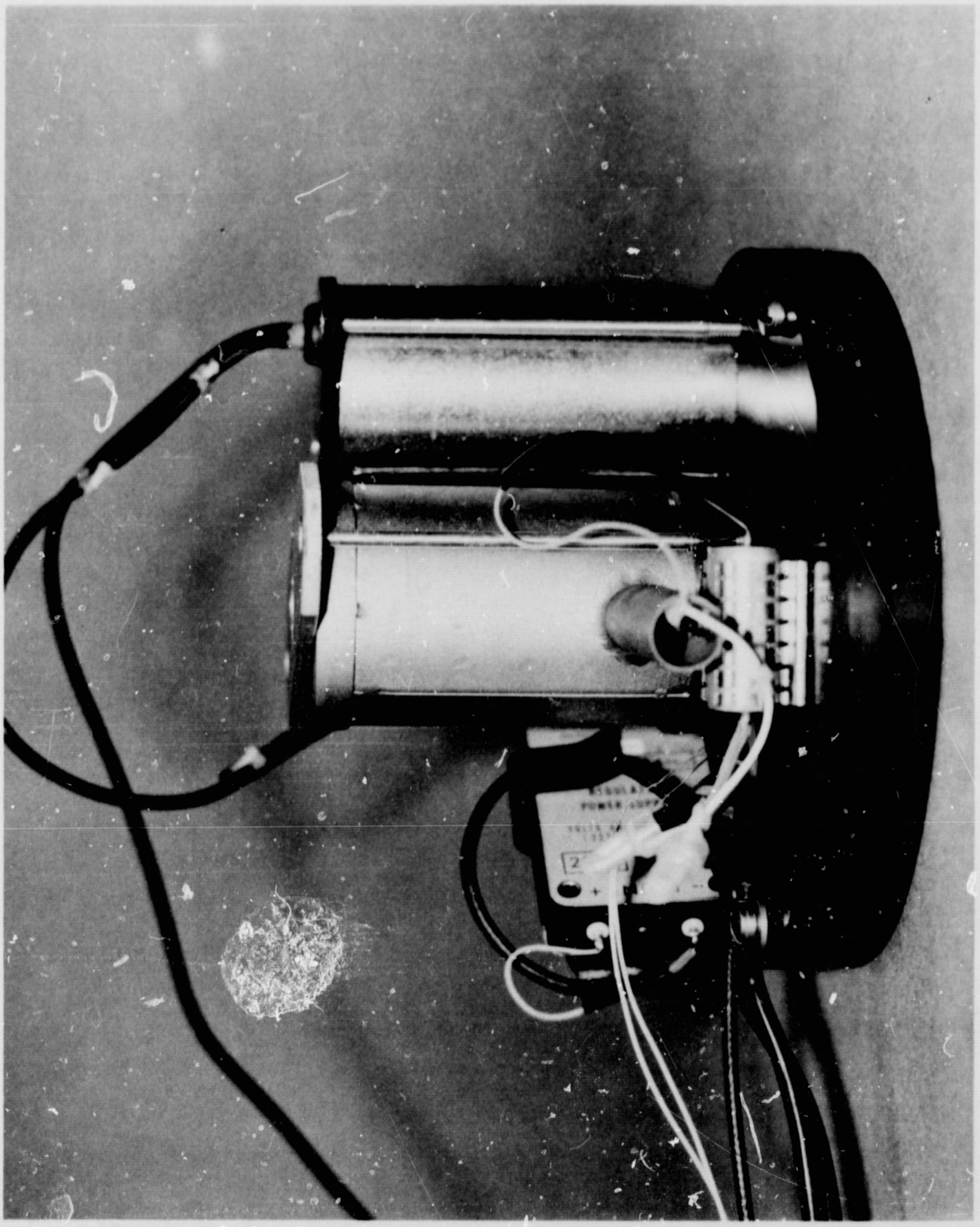

Figure 6 General View of Light Chopper

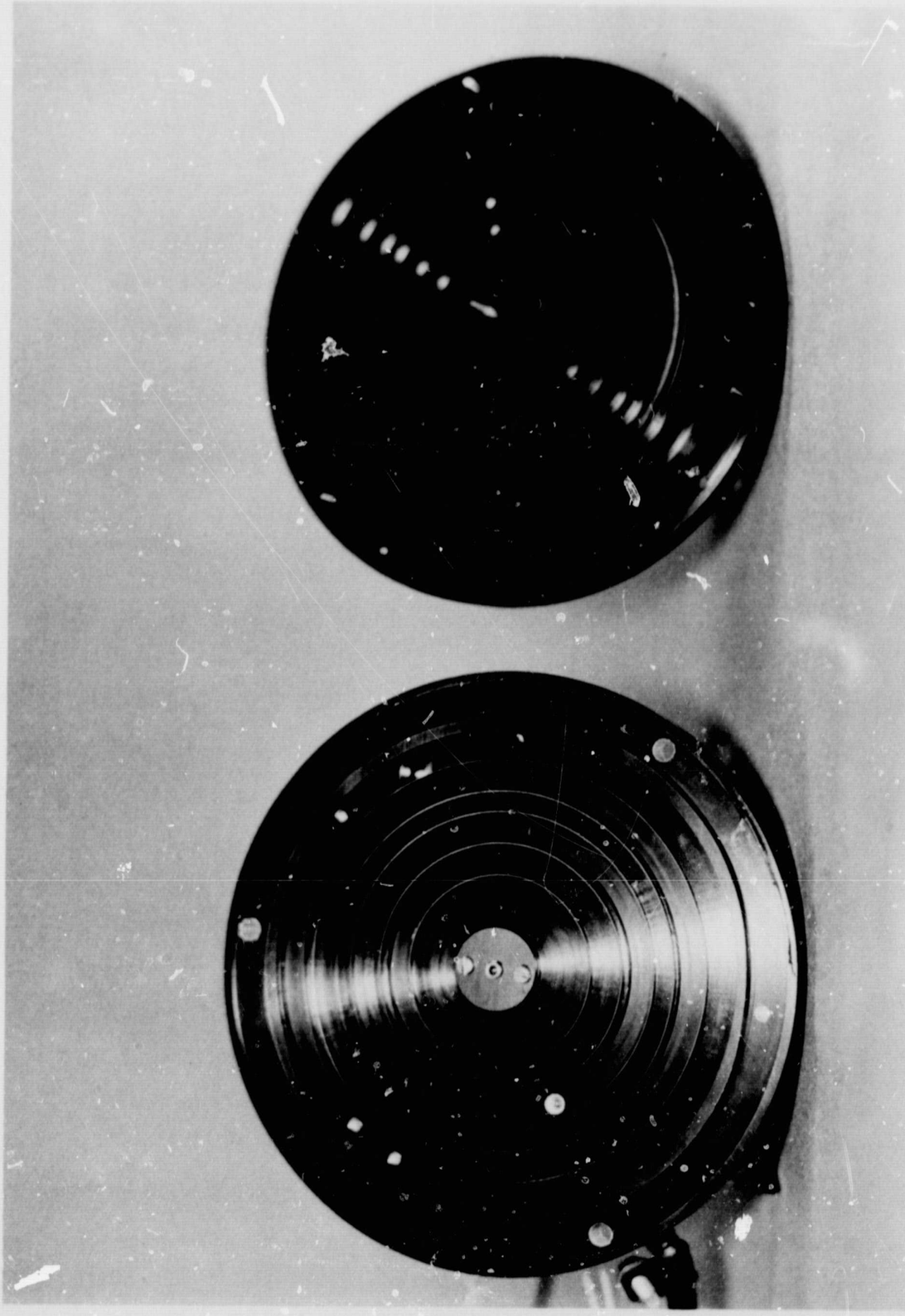

Figure 7 Light Baffles

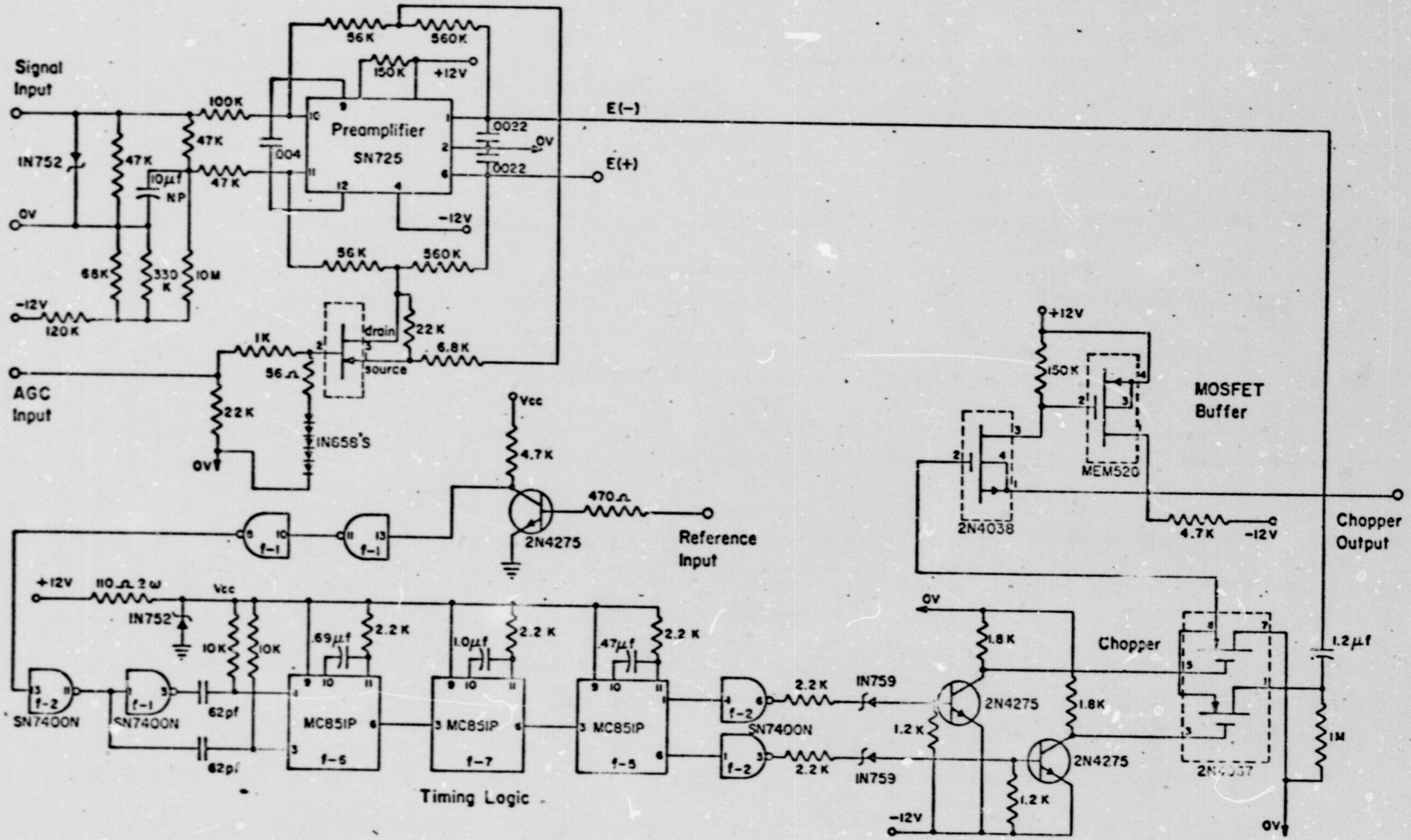

PHOTO MULTIPLIER PREAMP
WITH AGC AND CHOPPER

Figure 8 Telescope Electronics

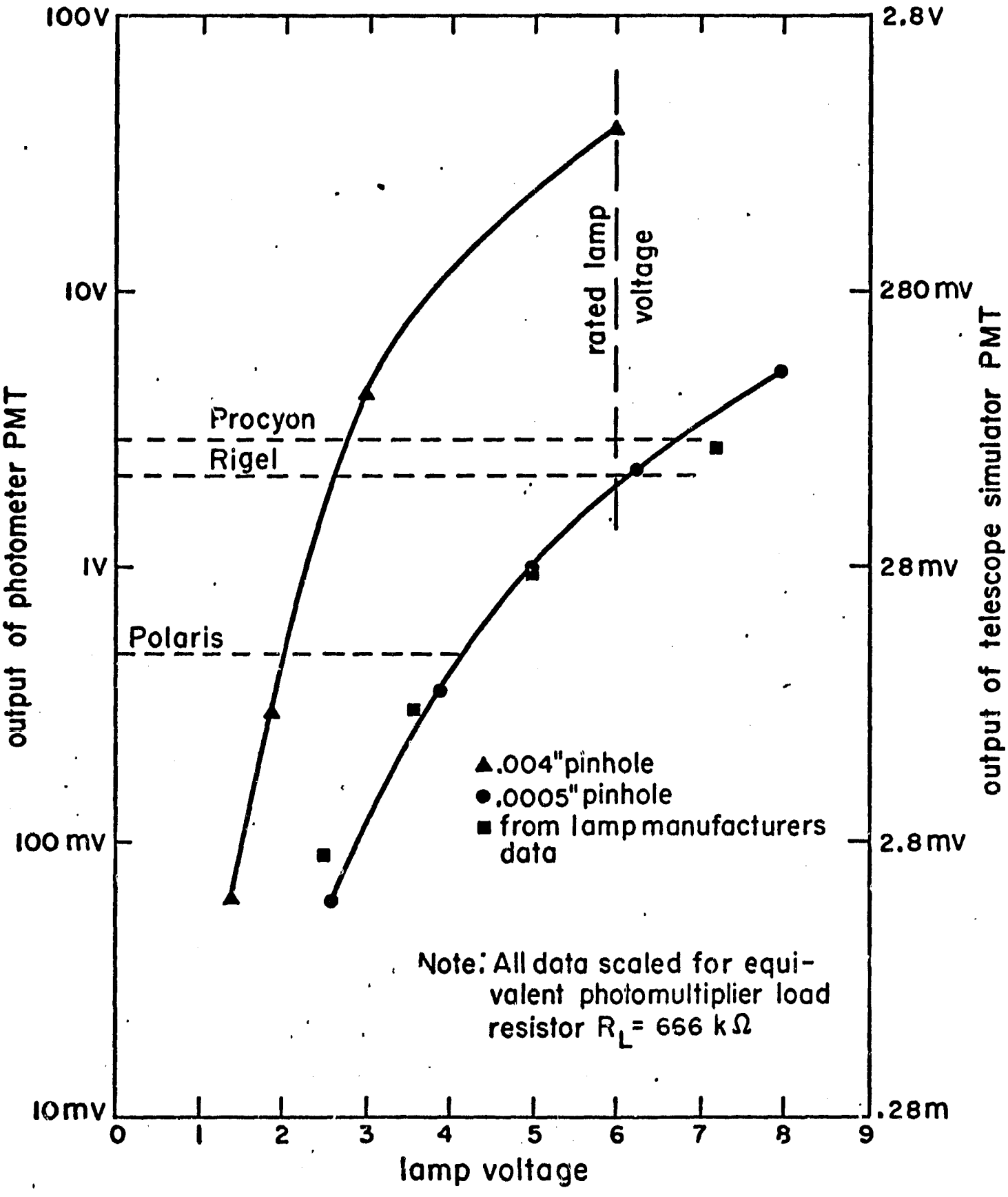

Figure 9 Star Simulator Calibration

Fig. 10 Comparison of observed noise with theoretical photon noise

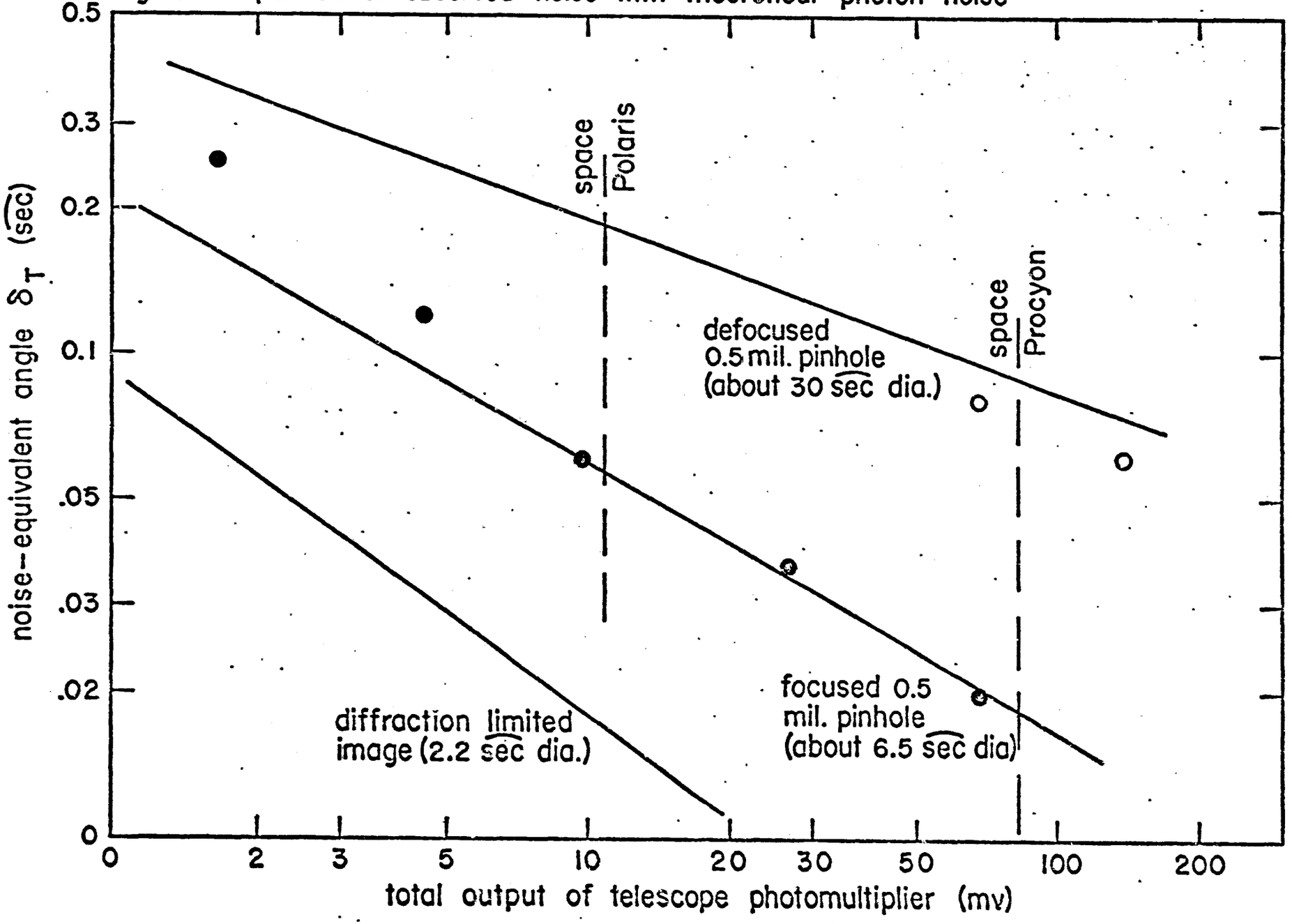

Fig.11 Focused image: linearity of central portion

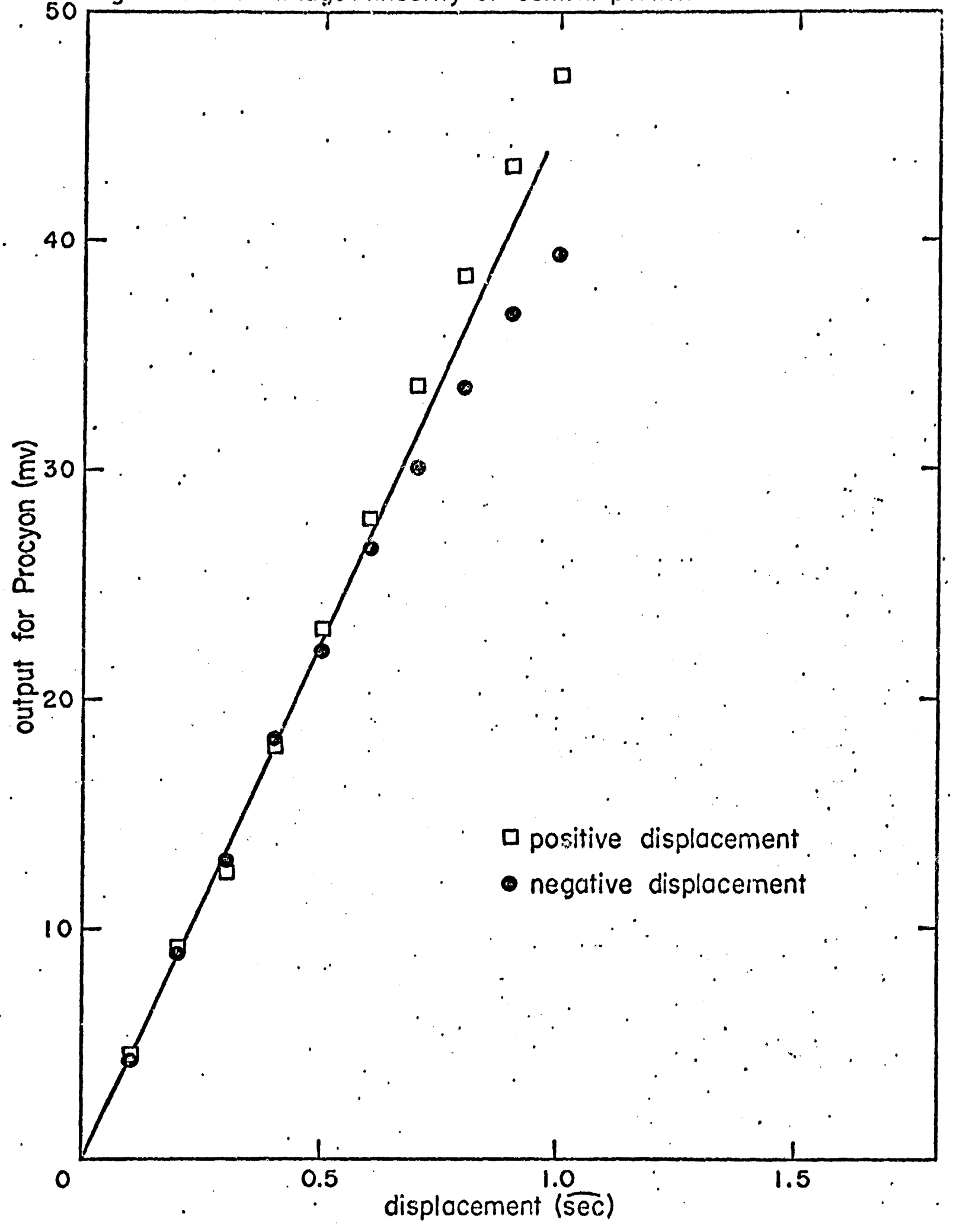

Fig. 12 Defocused image: linearity of central portion